A STUDY ON GTO TURN-OFF FAILURE MECHANISM

Hiromichi Ohashi and Akio Nakagawa

Toshiba Research and Development Center
1, Komukai Toshiba-cho, Saiwai-ku, Kawasaki 210, Japan

ABSTRACT

An infrared microscopic technology and exact one dimensional model were employed to clarify the processes which lead GTO to the gate turn-off failure. As a result of investigations, it was found that anode current density J_a in the current crowding region is influenced by anode voltage e_a. It finally increases approximately in the form of $J_a = K \cdot e_a$ (K:Constant), accompanying temerature rise ΔT in the N-base region, which is proportional to $\int e_a^2 \, dt$.
Influences of device design parameters and external circuit conditions on the GTO turn-off failure were well explained by taking the constant K and allowable maximum temperature rise $\Delta T(max)$ into account. The safe operation area concept for a high power GTO snubber circuit design was quantitatively established, using the above results as a design criterion.

INTRODUCTION

Although a gate turn-off (GTO) thyristor recently received much attention in regard to power conversion equipment applications, exact explanations have not been made for the gate turn-off failure. It is important to understand the gate turn-off failure in detail, not only for device design, but also from a GTO application point of view.
The purpose of this paper is to clarify the processes which lead the GTO to the gate turn-off failure, introducing an infrared microscopic technology and an exact one dimensional model. Influences of device design parameters and external circuit conditions on the failure were also discussed.

CURRENT CROWDING OBSERVATIONS

Figure 1 shows a diagram of the infrared observation system with an infrared radiometer, which is able to measure infrared light intensity due to direct carrier recombination and thermal radiation from the current crowding region. As is shown in the figure, the infrared radiation was observed from two directions with 20 microns space resolution.

Changes in the conduction region were measured through many 30 micron windows formed within a cathode electrode for detecting infrared radiation.
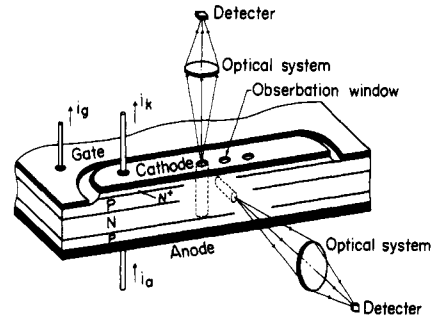

Fig.1 Infrared observation system.

Typical experimental results are shown in Fig.2. As a result of these investigations, it was found that conduction area squeezing toward the center of a rectangular emitter finger along the width direction is completed at least until the end of storage time. If anode current density J_a at the beginning of the fall time is below a certain value J_{ac} (around 400A/cm^2 for the sample under test), the conduction area remains constant during fall time. In other words, anode current density J_a reduces proportionally with the totoal anode current.
In the next step, current conduction area during fall time begins to reduce rapidly in the emitter length direction, once J_a exceeds J_{ac}, keeping conduction width almost constant.
Temperature and recombination radiation distributions along the GTO vertical direction, at the point where current crowding remains until the end of fall time, were measured under the condition of $J_a \gg J_{ac}$. As is obvious from Fig.3 (a), two kind of temperature peak were obtained. The first one, T_1, occurs just after the fall time, temperature peak point near junction J_2 to a point near junction J_1 in the N-base region. The second one, T_2, is generated around J_2 several tens of microseconds after the fall time. Since the conduction area width during fall time remains almost constant, the change in J_a due to current crowding in the length direction is related to radiation intensity due to recombination, emitted from the cross sectional side of the sample. Figure 3(b) shows recombination radiation distributions for the sample for the same driving conditions as for Fig.3(a).
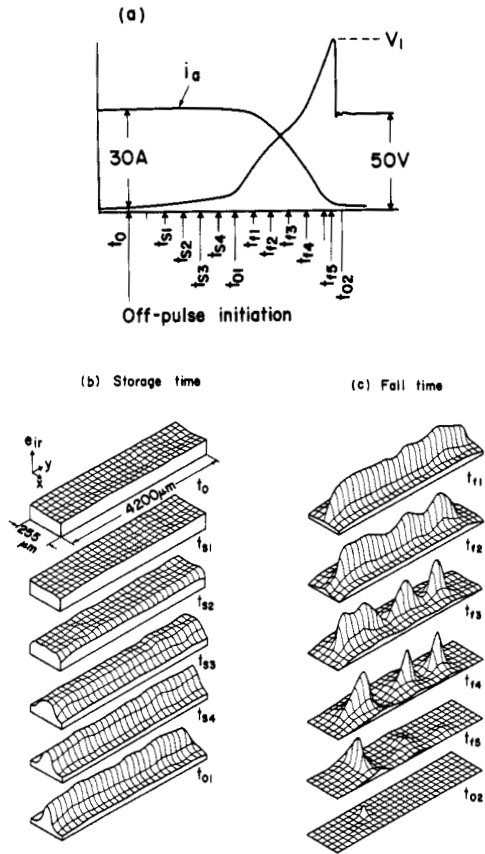
Fig.2 Changes in conduction area during storage time and fall time.

The measured relation between radiation intensity e_{ir} emitted from J_3 and anode voltage e_a for various conditions of gate turn-off anode current I_{ATO} are shown in Fig.4.

According to the numerical calculation results, anode current density J_a is proportional to excess carrier density n, at junction J_3 and e_{ir} at high injection level is given by $e_{ir} \propto n^2$.[1] Thus, J_a is written as follows,

$$J_a \propto \sqrt{e_{ir}} \quad . \qquad (1)$$

The relation J_a and e_a are obtained using Eq.(1) and experimental data on e_{ir} vs. e_a. Relations are shown by a dashed line in Fig.4.

As is obvious in the figure, J_a is influenced by anode voltage e_a and finally increases in the form of

$$J_a = K \cdot e_a \quad (K:Constant), \qquad (2)$$

accompaning temperature rise $\triangle T$ in the N-base region, which is proportional to

$$\triangle T = \frac{K}{W_{NB}(eff) \rho \cdot \gamma} \int e_a^2 \, dt \, , \qquad (3)$$

where $W_{NB}(eff)$: effective N-base width, ρ :specific

density and γ : spesific heat. $\triangle T$ corresponds to T_1 in Fig.3(a). According to the present experimentations, when T_1 exceeds around 300°C, gate turn-off failure was observed. These experimental results imply that gate turn-off failure can be controlled by making K as small as possible.
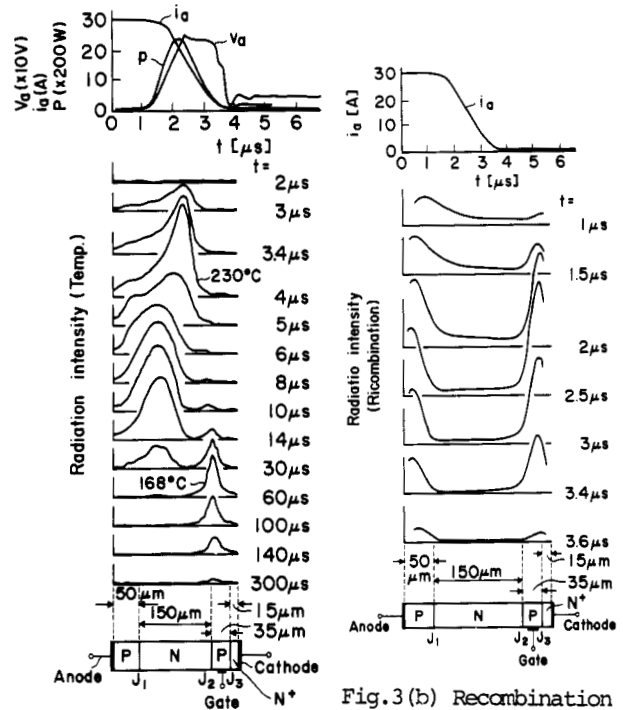

Fig.3(a) Temperature distributions
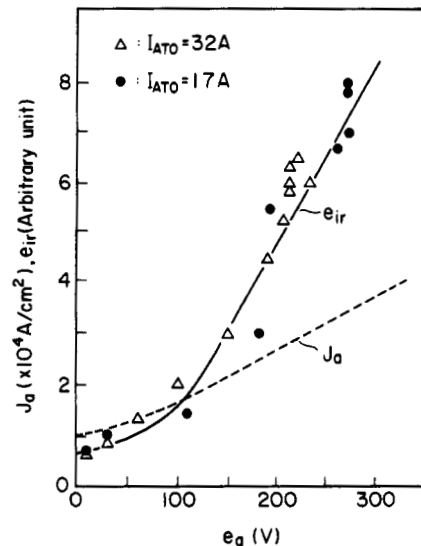

Fig.3(b) Recombination radiation distributions

Fig.4 Experimentally obtained anode current density as a function of anode voltage

17.3

EXACT ONE DIMENSIONAL MODEL

An exact one dimensional model for the turn-off processes will be presented in this section. The model includes Heavy doping effect,[2] Auger recombination,[3] carrier to carrier scattering,heat flow equation [4] and temperature dependent mobility.[5]
The simplified model for numerical calculation is shown in Fig.5. As is obvious from the current crowding observations, the conduction area width keeps almost constant, after it reaches a certain value, which is considered to be carrier diffusion length.[6]
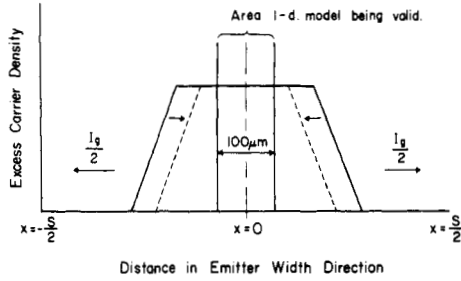
Fig.6 Simplified conduction area model

The exact one dimensional model is applied to this narrow final conduction area (100um for the sample used). Since the conduction area is assumed not to be affected by the negative gate current, while the conduction area is being squeezed, negative gate current influence on the area begins after the conduction width becomes almost constant. An anode voltage is externally given as an input data, taking the experimental data into consideration.
The change in anode current density J_a, which corresponds to the experimental results shown in Fig.4 were calculated and are illustrated in Fig.6, showing that negative gate current for the experimental results ranges from 600A/cm^2 to 1000A/cm^2.
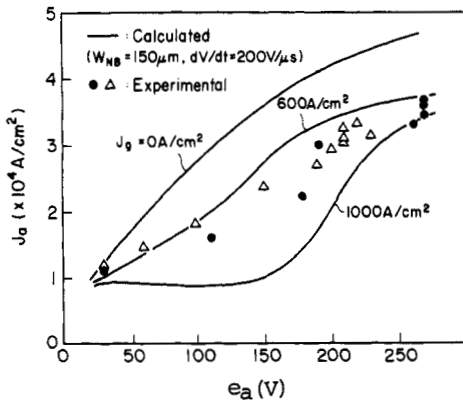
Fig.7 Calculated relations between J_a and e_a

Figure 7 shows one of the carrier distributions for the current crowding area during fall time. The current flows, exhausting the stored charge in the N-base region. The location, where carrier density in the N-base is minimum, moves from near J_2 to near J_1 in the N-base region, explaining the results shown

in Fig.3(b) well. All of these results,calculated by the exact one dimensional model, well explain the experimental results described in the previous section.

DISCUSSION

First of all, the meaning of the relation between J_a and e_a for the current crowding area will be discussed.
When carrier injection into the P-base region exceeds around 10^{18} cm^{-3} at the beginning of current crowding phenomenon, a reduction in current amplification factor for NPN transistor portion α_{npn} begins accompanying excess carrier exhaustion near J_2 in the N-base, as is shown in Fig.7.
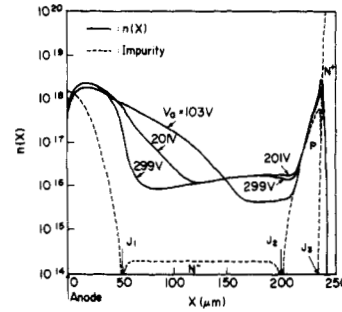
Fig.7 Calculated carrier distributions

Moreover, the negative gate current influence on the current crowding area accelerates the carrier exhaustion. Consequently, a high electric field appears in the region nearby. Electric field distribution variation, which corresponds to the results shown in Fig.3, were calculated and illustrated in Fig.8.
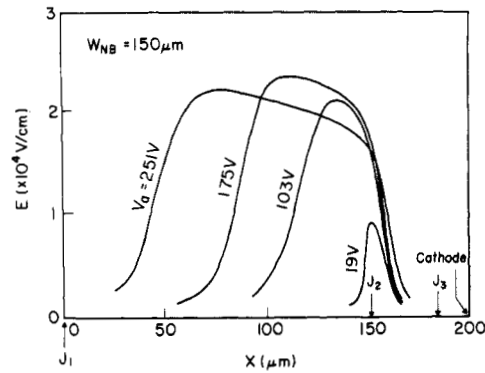
Fig.8 Calculated electric field distributions

Since current flow in the high electric field region is mainly transported by drift current, the condition $\mu_n/\mu_p \sim J_n/J_p$ is applicable to the high electric region, where μ_n, μ_p : electron and hole mobility and J_n, J_p : electron and hole current density. The ratio μ_n/μ_p becomes identical with J_n/J_p when electric field E reaches around

17.3

$1 \sim 2 \times 10^4$ V/cm, in accordance with anode voltage increase, because μ_n/μ_p reduces with increase in E. Further increase in anode voltage e_a causes high electric field region expansion, keeping an almost constant electric field. As is obvious from Fig.7 anode current flow is mainly determined by the hole diffusion current from the P-emitter region, while high electric field region due to higher anode voltage causes high anode current density.

According to numerical calculation, it was confirmed that the relations between J_a and e_a are greatly influenced by N-base width, P-base sheet resistivity, anode voltage waveforms and the negative gate driving conditions. All of these parameters show close relations with maximum gate turn-off anode current I_{ATO}(max).[7],[8]

Hereafter, consider gate turn-off failure for a high power GTO, whose cathode is highly inter-digited, consisting of many narrow emitter fingers surrounded by a gate region. According to the experimental results shown in Fig.2, it can be assumed that, as long as anode current for each emitter finger is kept under J_{ac}, rather good current balance between emitter fingers is maintained. However, further increase in the emitter finger current causes drastic current crowding into a few emitter fingers, accompanied by GTO turn-off failure.

For simplicity, the anode voltage waveform during the fall time is formulated as,

$$e_a = \frac{V_1}{T_f} \cdot t \qquad (4)$$

where V_1: anode voltage at the end of the fall time, T_f: fall time and t: time. Substituting Eq.(4) into Eq.(3) yields ΔT.

$$\Delta T = \frac{K \cdot V_1^2 \cdot T_f}{3 \cdot W_{NB}(\text{eff}) \cdot \rho \cdot \gamma} \qquad (5)$$

The numerical calculation show that constant K is approximately in inverse proportion to W_{NB} ($K=C_1/W_{NB}$) and W_{NB}(eff) is assumed to be W_{NB}(eff)= $C_2 \cdot V_1$. Thus, Eq.(5) is rearranged as,

$$V_1 = (\frac{3 \cdot \Delta T \cdot C_2 \cdot \rho \cdot \gamma}{C_1 \cdot T_f}) \cdot W_{NB} \qquad (6)$$

Figure 9 shows experimentally obtained relations between W_{NB} and V_1(max) when turn-off failure
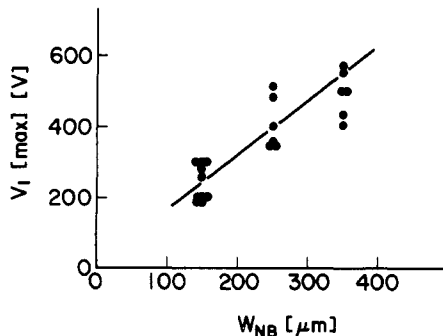
Fig.9 Experimentally obtained relations between W_{NB} and V_1(max)

occurs, showing approximately linear relation between them. Since the experimentations were carried out under almost the same T_f conditions ($T_f=2 \sim 3\mu s$), it is obvious from Eq.(6), that the failure occurs when ΔT exceeds allowable maximum temperature ΔT(max) for safe opperation. When ΔT(max) and T_f are assumed to be $300°C$ and $2.5\mu s$ respectively, the Eq.(6) constant proportion becomes about 2×10^4. This value shows good agreement with the slope of the experimental results shown in Fig.9 in order.

V_1(max) will become one of the important factors for snubber circuit design. Fig.10 shows the relation between the snubber capacitance value and I_{ATO}(max). A safe operating area is calculated using the newly developed snubber circuit calculation model, which takes into account V_1(max). The calculated safe operating area explains the gate turn-off failure. All of the experimentally obtained failure points, except one, are located outside the calculated safe operating area.
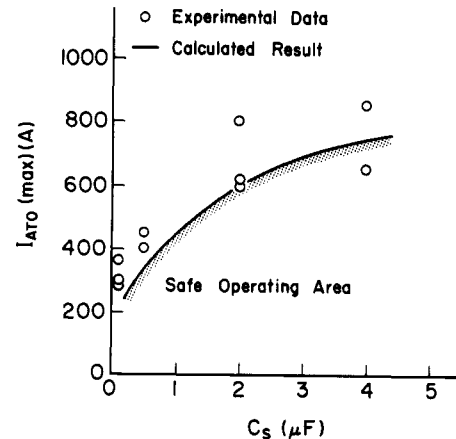
Fig.10 Calculated safe operating area

In summary, influences of device design parameters and external circuit conditions on the GTO turn-off failure were well explained taking into account the relation written by Eq.(2) and ΔT(max).

REFERENCES

1) H. Schlangenotto et al.: IEEE Trans., ED-26(1979)191
2) A. Nakagawa: Solid-St Electron,22(1979)943
3) A. Nakagawa et al,: IEEE Trans.: ED-28(1981)231
4) M. Adler: IEEE Trans.: ED-25(1978)16
5) E. Alwin et al.: IEEE Trans., ED-24(1977)1297
6) E. Wolley: IEEE Trans., ED-13(1966)590
7) M.Azuma et al.: 1979IEDM Tech. Digest,246
8) H. Ohashi et al.: Toshiba Review, 112(1977)23

17.3